CHEMISTRY OF MATERIALS

Article

pubs.acs.org/cm

# Combining Fast Li-Ion Battery Cycling with Large Volumetric Energy Density: Grain Boundary Induced High Electronic and Ionic Conductivity in $Li_4Ti_5O_{12}$ Spheres of Densely Packed Nanocrystallites

Chao Wang,[†,∥,⊥] Shuan Wang,[†,⊥] Yan-Bing He,[*,†] Linkai Tang,[†,∥] Cuiping Han,[†,∥] Cheng Yang,[†] Marnix Wagemaker,[*,‡] Baohua Li,[*,†] Quan-Hong Yang,[†] Jang-Kyo Kim,[§] and Feiyu Kang[†,∥]

[†]Engineering Laboratory for the Next Generation Power and Energy Storage Batteries, Graduate School at Shenzhen, Tsinghua University, Shenzhen 518055, P.R. China

[‡]Department of Radiation Science and Technology, Delft University of Technology, Mekelweg 15, 2629JB Delft, The Netherlands

[§]Department of Mechanical and Aerospace Engineering, The Hong Kong University of Science and Technology, Hong Kong, P.R. China

[∥]Laboratory of Advanced Materials, Department of Materials Science and Engineering, Tsinghua University, Beijing 100084, P.R. China

Supporting Information

**ABSTRACT:** One of the key challenges toward high-power Li-ion batteries is to develop cheap, easy-to-prepare materials that combine high volumetric and gravimetric energy density with high power densities and a long cycle life. This requires electrode materials with large tap densities, which generally compromises the charge transport and hence the power density. Here densely packed $Li_4Ti_5O_{12}$ (LTO) submicrospheres are prepared via a simple and easily up-scalable self-assembly process, resulting in very high tap densities (1.2 g·cm$^{-3}$) and displaying exceptionally stable long-term high rate cyclic performance. The specific capacities at a (dis)charge rate of 10 and 20 C reach 148.6 and 130.1 mAh g$^{-1}$, respectively. Moreover, the capacity retention ratio is 97.3% after 500 cycles at 10 C in a half cell, and no obvious capacity reduction is found even after 8000 cycles at 30 C in a full $LiFePO_4$/LTO battery. The excellent performance is explained by the abundant presence of grain boundaries between the nanocrystallites in the submicron spheres creating a 3D interconnected network, which allows very fast Li-ion and electron transport as indicated by the unusually large Li-ion diffusion coefficients and electronic conductivity at ($6.2 \times 10^{-12}$ cm$^2$ s$^{-1}$ at 52% SOC and $3.8 \times 10^{-6}$ S cm$^{-1}$, respectively). This work demonstrates that, unlike in porous and nanosheet LTO structures with a high carbon content, exceptionally high rate charge transport can be combined with a large tap density and hence a large volumetric energy density, with the additional advantage of a much longer cycle life. More generally, the present results provide a promising strategy toward electrode materials combining high rate performances with high volumetric energy densities and long-term cyclic stability as required for the application in electric vehicles and tools.

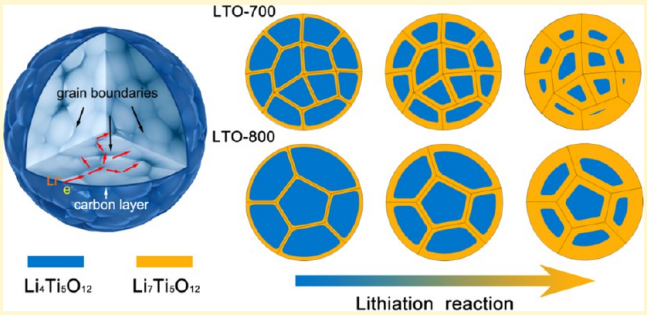


## INTRODUCTION

The development of power sources for pure or hybrid electric vehicles (EVs) and renewable energy systems has been considered as one of the most important issues to solve the energy crisis in the 21st century.[1] In the pursuit to solve this issue, lithium-ion batteries (LIBs) have been intensively studied due to their relatively high energy density. However, the relatively poor safety, limited cyclic life, inferior high rate charge, and poor low temperature properties are often considered as the most critical issues of LIBs to be solved. Conventional carbon-based anodes lead to accumulative formation of irreversible lithium dendrites on the carbon electrode surface, especially upon fast charging, long-term cycling, or low-temperature charging conditions. In turn, the dendrite formation on the carbon anode will lead to severe safety hazards.[2−4] This has motivated a myriad of investigations that have been hitherto conducted aiming at the development of new electrode materials having improved electrochemical and safety performances.[5,6]

One of the most promising alternative anode materials for high-rate LIBs is spinel $Li_4Ti_5O_{12}$ (LTO) based on its excellent cyclic reversibility (a consequence of almost zero structural volume change during Li ion insertion/extraction), high safety, and good Li-ion kinetics at low temperatures.[7−10] In addition,

Received: May 29, 2015
Revised: July 8, 2015
Published: July 8, 2015





DOI: 10.1021/acs.chemmater.5b02027
Chem. Mater. 2015, 27, 5647−5656

the very flat voltage plateau, close to 1.55 V versus $Li^+/Li$, is higher than the reduction potential of most organic electrolytes, effectively deterring the formation of solid electrolyte interface (SEI) films.[11−13] As a consequence, LTO is considered to be much safer and stable than carbon-based anodes. Despite the above-mentioned advantages, one of the major challenges is to develop electrodes that combine a high power density with a higher energy density. The poor electronic and ionic conductivities of LTO[14−16] have initiated the development of many types of nanostructured LTO materials, such as nanoscale porous frameworks,[17] nanosheets,[12,18] arrays[19,20] and mesoporous hollow spheres,[21] aiming at larger reaction surface areas and shortened Li-ion and electron transport lengths. However, the large specific surface area of the nanostructured LTO materials compromises the tap density of the LTO powders,[22,23] which decreases the volumetric energy density of the full cells. Besides, these nanostructured LTO materials are normally synthesized on the basis of hydrothermal and solvothermal synthetic methods, which hinder the practical mass productions and applications.[18,24] Therefore, various approaches have been developed to prepare secondary microsized and porous LTO secondary spheres consisting of nanosized primary particles to achieve high tap densities in combination with high-rate electrochemical performance.[16,18−20,22] Up to date, this appears challenging, in particular in combination with cheap and up-scalable preparation methods as illustrated by Table S1, which presents a summary of some of the reported preparation methods of secondary LTO microspheres, typically using spray-drying and hydrothermal processes,[18,19] in combination with their performances. It should be noted that also the electrode loading influences the capacity retention at increased rates,[25−27] which is however not often reported. Most of the reported preparation strategies require high energy consumption and high cost, which are unfavorable for mass production and precise structural control. Therefore, it is urgently necessary to develop methods to synthesize LTO materials that combine small surface areas, high tap densities without compromising the electronic and ionic conductivities.

In this paper, a facile one-pot way is developed to synthesize LTO compact submicrospheres by self-assembly of nanocrystals. The hexadecylamine (HDA) is used as a capping and condensing agent to induce and promote the formation of $TiO_2$ spheres impregnated with Li ions from the amorphous primary $TiO_2$ particles and Li ions. Consequently, these spheres were calcinated to form LTO spheres fortified by densely packed primary LTO nanocrystals. No spray-drying or hydrothermal processes are involved in this method, making this method cheap and easy to scale up. The obtained highly compacted LTO spheres are submicrosize, about 500 nm, and have a high tap density. The as-prepared spheres show very large Li-ion diffusion coefficients at 52% SOC ($6.2 \times 10^{-12}$ $cm^2$ $s^{-1}$) and electrical conductivities ($3.8 \times 10^{-6}$ S $cm^{-1}$), responsible for the exceptionally high rate capabilities and cyclic stability. As shown in Table S1 in the Supporting Information (SI), the LTO submicrosphere obtained in this work delivers significantly improved specific capacities in combination with high tap densities, especially at high (dis)charge current densities, compared to other reported LTO electrodes. The nanosized carbon coating and the abundance of phase boundaries in the compact LTO spheres are expected to be responsible for the excellent Li-ion and electron transport inside the LTO spheres. Full batteries were assembled using $LiFePO_4$ (LFP) as cathode material and the prepared LTO spheres as anode material, which achieve ultrahigh rate performance and excellent cyclic stability. No significant capacity fading is found even after 8000 cycles at 30 C (dis)charge rate. The developed high volumetric energy density LTO anodes, suitable for cheap mass production, not only pave the way toward high-rate Li-ion batteries with excellent cycle life, it additionally provides new general insights for the synthesis of electrode materials combining high tap density and high rate capabilities as required for the lithium ion power batteries.

## RESULTS AND DISCUSSION

The LTO spheres were prepared by dissolving 16 mL of titanium(IV) butoxide (TBT) into 200 mL of absolute ethanol followed by magnetic stirring for 30 min. Subsequently, the transparent TBT solution was added by 4.03 g of lithium acetate (LiAc) and 2.0 g of hexadecylamine (HDA), where HDA was used as a structure-guiding agent in the formation of amorphous $TiO_2/Li^+$ spheres. Next, 5.5 mL of $NH_3{\cdot}H_2O$ (25%) was dropwise added to the precursor solution under constant magnetic stirring for the hydrolysis of TBT. After 2 h of stirring, the transparent solution gradually turned into a milky liquid. The solution was dried at 80 °C for 24 h to obtain the white powder of amorphous $TiO_2/Li^+$ spheres. Finally, this white powder was further annealed at different temperatures of 600, 700, and 800 °C for 7 h in an Ar flow to obtain the final gray LTO powder (denoted as LTO-600, LTO-700, and LTO-800, respectively). The detailed synthesis procedures are illustrated in Figure 1. First, the dissolved TBT in ethanol

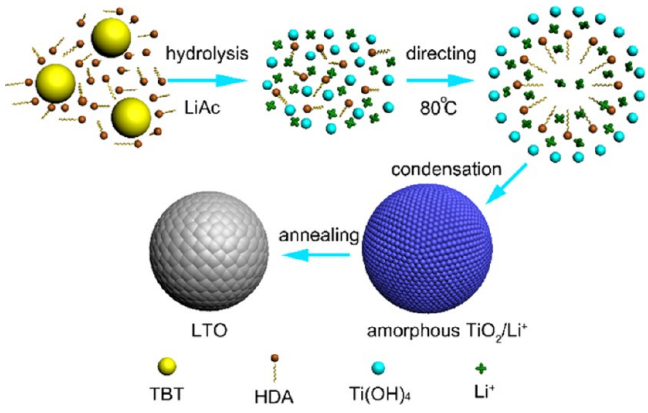


**Figure 1.** Schematic diagram of the formation process of the compact LTO spheres.

was hydrolyzed to $Ti(OC_4H_9)_{4-x}(OH)_x$ by adding $NH_3{\cdot}H_2O$ and further hydrolyzed to $Ti(OH)_4$. During heating at 80 °C, the $Ti(OH)_4$ gradually was condensed into amorphous $TiO_2$ particles, which were self-assembled to form amorphous $TiO_2$/lithium acetate secondary spheres with the aid of HDA. All these growth and self-assembly took place in an one-step process probably through a cooperative assembly process involving long-chain alkylamine and $Ti(OC_4H_9)_{4-x}(OH)_x$ species/oligomers.[28,29] The precursor spheres were annealed at different temperatures obtain LTO spheres.

The X-ray diffraction (XRD) analysis was used to identify the crystallographic structure of LTO spheres prepared at different temperatures (Figure 2a). It is found that the phase purity of products strongly depends on the annealing temperature. The XRD patterns of both LTO-700 and LTO-800 spheres are


DOI: 10.1021/acs.chemmater.5b02027
Chem. Mater. 2015, 27, 5647−5656

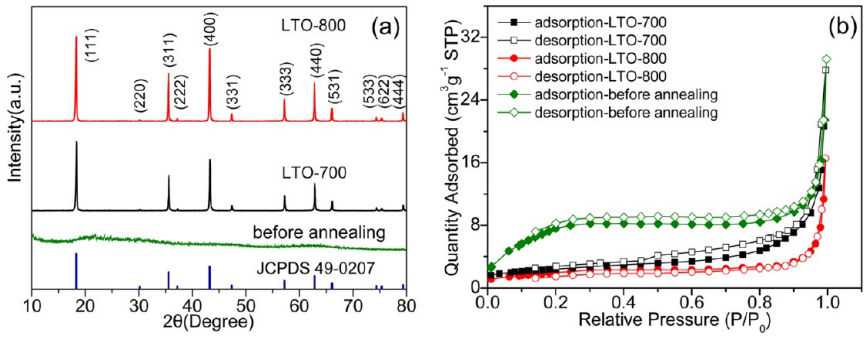


**Figure 2.** (a) X-ray diffraction (XRD) patterns and (b) nitrogen adsorption/desorption isotherms at 77 K of LTO before annealing, LTO-700 and LTO-800 spheres.

consistent with JCPDS card no. 49-0207 and can be indexed to the spinel structure of LTO with the space group Fd3m. For the 800 °C annealing temperature, the peak intensities clearly augment, indicating more and larger LTO crystalline material. In contrast, the LTO-600 spheres contain impure phases of $TiO_2$ and $Li_2TiO_3$ (Figure S1a in the SI), suggesting that the annealing temperature must be 700 °C or higher to ensure full transformation into highly crystalline LTO.

According to the nitrogen adsorption/desorption isotherms (Figure 2b), the Brunauere–Emmette–Teller (BET) specific surface areas are 24.4 and 25.5 $m^2\ g^{-1}$ for LTO spheres precursors and the LTO-600, respectively, and their corresponding pore volumes are 0.018 and 0.076 $cm^3\ g^{-1}$. When the annealing temperature increases from 600 to 700 and 800 °C, the BET surface areas of LTO-700 and LTO-800 remarkably decrease to 8.6 and 6.2 $m^2\ g^{-1}$, respectively, and their corresponding pore volumes reduce to 0.042 and 0.011 $cm^3\ g^{-1}$. These small BET surface areas and pore volumes demonstrate very dense structures with nearly no pores inside the LTO spheres before and after annealing resulting in very high tap densities. It is noted that the above BET surface areas are more than an order of magnitude lower compared to those previously reported on LTO spheres (Table S1 in the SI).

The morphologies and structures of the LTO spheres before and after annealing were examined by scanning electron microscopy (SEM) and high-resolution transmission electron microscopy (HRTEM), as shown in Figures 3 and 4. The spheres before annealing are 400–600 nm in diameter and contain much smaller (5–20 nm in diameter) primary amorphous $TiO_2$ particles impregnated with lithium acetate (Figure 3a,b). TEM images show that the precursor spheres are not hollow but exist as a solid amorphous structure (Figure 3c,d). The spheres obtained after annealing at different temperatures consist of densely packed primary LTO nanocrystals while maintaining uniform overall sphere diameters in the range of 400–600 nm (Figure 3e–h and S2a,b in the SI). It is worth noting that the primary LTO particle size changes drastically depending on the annealing temperature, growing from 36 to 42 and 55 nm in average diameter according to the Debye–Scherrer equation when the annealing temperature is increased from 600 to 700 and 800 °C, respectively. The morphologies of these spheres with in situ grown spinel LTO nanocrystals are very different from the secondary spheres consisting of loosely packed primary particles reported previously, as shown in Figure S3 in the SI. In contrast, LTO precursors without using HDA consists of irregular aggregates containing smaller primary amorphous $TiO_2$ particles (Figure S4 in the SI). After annealing, the obtained LTO is composed

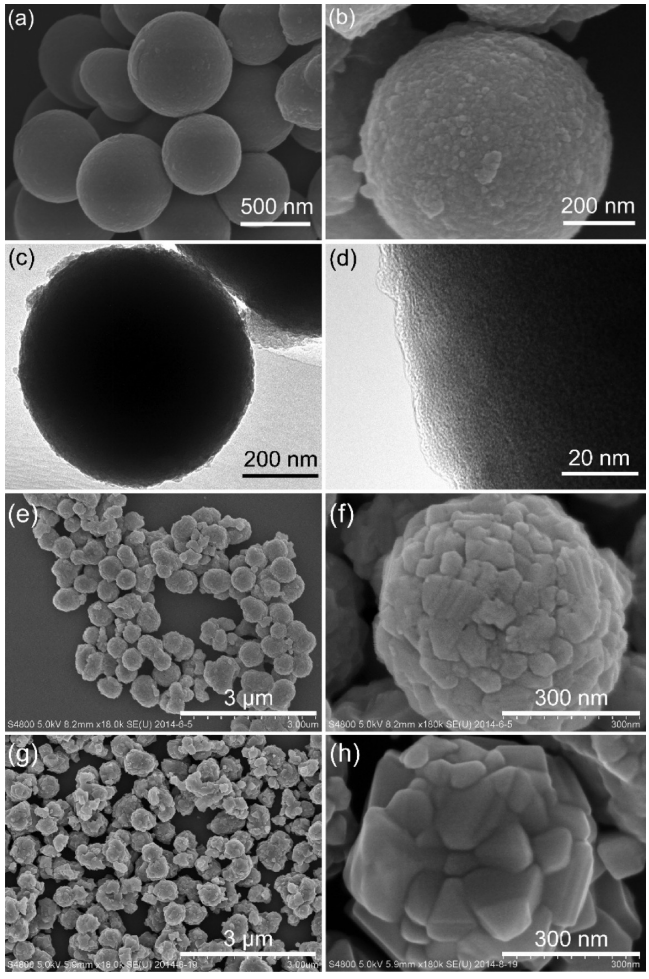


**Figure 3.** SEM (a, b) and HRTEM (c, d) images of LTO spheres before annealing and annealed at (e, f) 700 °C and (g, h) 800 °C.

of uniform single particles, which indicates that the HDA effectively guides the formation of the compact LTO spheres. We also used other organic amines and surfactants such as cetyltrimethylammonium bromide (CTAB) in the preparation of LTO, in which case single crystal lumps of LTO were formed, as shown in Figure S5 in the SI.

The HRTEM images in Figure 4 show that both LTO-700 and LTO-800 are neither hollow nor porous structures but rather solid clusters grown by compact spinel LTO nanocrystals (Figure 4a,c). They have a well-defined crystalline structure with a lattice plane spacing of 0.48 nm, which is consistent with


DOI: 10.1021/acs.chemmater.5b02027
Chem. Mater. 2015, 27, 5647–5656

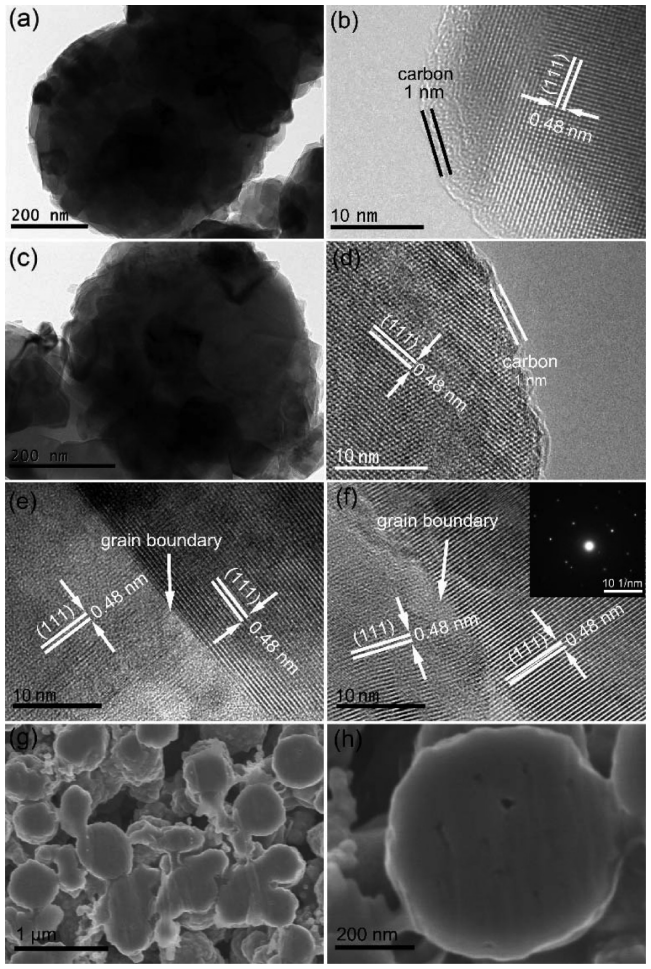


**Figure 4.** HRTEM images of LTO spheres synthesized at (a, b) 700 °C and (c, d) 800 °C. (e, f) Grain boundaries in the LTO-700 spheres where the inset in (h) shows the corresponding SAED pattern of a single crystallite grain. (g, h) The cross-sectional SEM images of LTO-700.

the (111) facet of spinel LTO (Figure 4b,d). The outmost nanocrystals of the LTO spheres are coated by a ∼1 nm thin carbon layer, which is probably originating from the HDA. Because the capping agent of HDA controlled the hydrolysis reaction of TBT and guided the self-assembly and condensation of the LTO precursors, this played a key role in the formation of uniform carbon layer on LTO nanocrystals. The cross-sectional images of LTO spheres further clearly illustrate the solid internal structure of the LTO spheres (Figure 4g,h). The electrical conductivity of LTO-700 spheres is measured to be $3.8 \times 10^{-6}$ S cm$^{-1}$, which is much higher than the intrinsic electronic conductivity $10^{-13}$ S cm$^{-1}$ of LTO.[12,20]

It may be anticipated that the uniform carbon layer is at least partially responsible for the increase in the electrical conductivity of the compact LTO spheres. In addition, we expect that the grain boundaries will increase the intrinsic LTO electrical conductivity, as will discussed below. The notably high electrical conductivity is of extreme importance for fast charge transfer throughout the surface of LTO spheres. According to the thermogravimetric analysis (TGA) and Raman spectra (Figure S6 in the SI), the carbon is in an amorphous state, and its content in LTO-700 spheres are estimated to be ∼0.4 wt %, which is much lower than 3−7 wt % for conventional carbon-coated LTO.[18,20,21] The carbon content of LTO-800 is slightly lower compared to that of LTO-700. The values of the ratio $I_D/I_G$ in the Raman spectra of LTO-700 and LTO-800 are 3.35 and 3.03, respectively, which demonstrates that the graphitization degree of amorphous carbon increases with increasing annealing temperature.[30,31] HRTEM and STEM images show that the nanocrystals are tightly grown together creating an abundance of grain boundaries (Figure 4e,f, Figure S7 in the SI) as opposed to LTO-800 existing of larger crystallites. The corresponding selected area electron-diffraction (SAED) pattern of a nanocrystal in the inset of Figure 4f shows that the nanocrystal is a single crystalline LTO grain with a well-defined crystalline structure. No carbon coating layer is observed on the boundaries of nanocrystals, which indicates that the carbon coating layer is only formed on the surface of outmost nanocrystals. Owing to the unique dense structure and the very low carbon content leads to the high tap density of LTO-700 spheres reaching 1.2 g cm$^{-3}$, which is twice that of the carbon-coated and nanoscale LTO (∼0.6 g cm$^{-3}$).[20]

The electrochemical properties of the annealed LTO spheres were evaluated using half-coin cells, as shown in Figure 5. Prior to the rate-dependent cycling, the LTO-700 and LTO-800 electrodes are subjected to three formation cycles using a 0.1 C rate (Figure S8 in the SI). The columbic efficiency of the first cycle for LTO-700 and LTO-800 are 96.13% and 96.32%, respectively. The relatively low columbic efficiency may be attributed to lithium ions that are trapped within the grain boundary regions during the initial (dis)charge cycles. The (dis)charge profiles are presented of the LTO-700 electrode at different current rates from 0.1 to 30 C in the voltage range of 1.0−2.5 V (Figure 5a). At a low C-rate (e.g., 0.1 C), the electrode delivers a remarkable specific capacity of 174.8 mAh g$^{-1}$, which is very close to the theoretical capacity of 175 mAh g$^{-1}$. As the current rate is increased from 1 to 5 and 10 C, the specific capacities only slightly decrease from 170.1 to 158.5 and 148.6 mAh g$^{-1}$, respectively (Figure 5c). Even at very high rates, 20 and 30 C, the specific capacities remain as high as 130.1 and 119.6 mAh g$^{-1}$, respectively, corresponding to 74.4% and 68.4% of that at 0.1 C. It is also worth noting that the (dis)charge overpotentials for the LTO-700 at 10 and 30 C are 0.192 and 0.424 V respectively, very similar to that of LTO nanosheets.[18] This small polarization indicates very low internal resistance for electron and Li-ion transport in the LTO-700 spheres in line with the excellent lithiation and delithiation behavior during the high rate cycling.

Figure 5d clearly shows that the densely packed LTO-700 spheres deliver an exceptional specific capacity of 144.5 mAh g$^{-1}$ − equivalent to 97.3% capacity retention−even after 500 cycles at a high current density of 10 C, proving their excellent (de)lithiation kinetics and reversibility. The specific capacity and capacity retention values obtained at 10 C are among the highest ever reported for LTO spheres containing loosely packed primary particles, as shown in Table S1. The morphologies and the Fourier transform infrared spectra (FTIR) of the LTO-700 electrodes before and after 500 cycles at 10 C are shown in Figures S9 and S10 in the SI, which demonstrates the high structural stability of the compact LTO spheres during the high rate cycling tests. The $Li_2CO_3$ (at 864, 1427, and 1497 cm$^{-1}$) and $ROCO_2Li$ (at 1624 cm$^{-1}$) species were formed on the surface of the cycled LTO spheres, which may be attributed to the interfacial reactions between the LTO and electrolyte solution.[32−34] The excellent rate and cycling performance of LTO-700 suggests that the formation of Li


DOI: 10.1021/acs.chemmater.5b02027
Chem. Mater. 2015, 27, 5647−5656

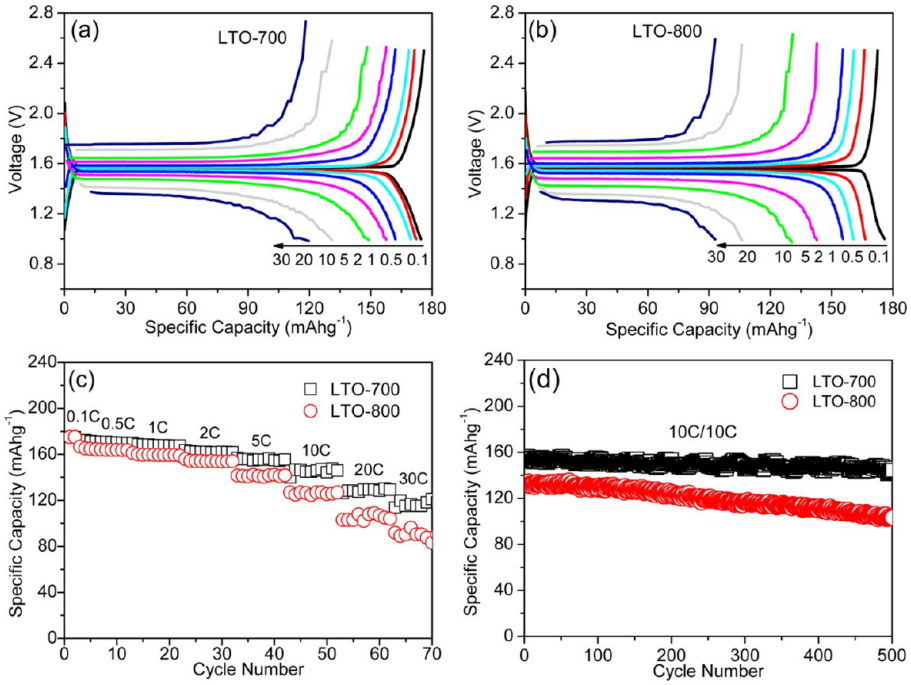


**Figure 5.** Electrochemical properties of LTO spheres annealed at 700 and 800 °C: (a, b) (dis)charge curves, (c) specific capacities at different C rates, (d) cyclic performance at a rate of 10 C.

carbonate on the surface of the compact LTO spheres does not influence their performance. As the annealing temperature increases to 800 °C, the capacity of the LTO-800 electrode reduces by 14% compared to LTO-700 at 10 C and further drops to 91.1 mAh $g^{-1}$ at 30 C (Figure 5b). Similarly, the rate capabilities and cyclic stability of the LTO-800 electrodes are marginally inferior to the LTO-700 electrodes (Figure 5c,d). The specific capacity of the LTO-800 electrode decreases from 132.3 to 104.5 mAh $g^{-1}$ with a capacity loss of 21.0% after 500 cycles at 10 C. The results indicate that the increase of LTO nanocrystal size inside the compact submicron spheres is detrimental for the rate and cycling performance. The electrochemical performance of the LTO material calcined at 600 °C also has been evaluated. Compared to the LTO-700 material, LTO-600 shows poor electrochemical performance as demonstrated by the low specific capacity at 10 C of only 43.8 mAh $g^{-1}$ (Figure S11 in the SI), which may be attributed to the presence of $Li_2TiO_3$ as impurity phase.

The cyclic voltammetry (CV) profiles were measured to clarify the kinetic behavior of the annealed LTO spheres (Figure S12 in the SI). The CV curve of LTO-700 has two sharp, symmetrical redox peaks at 1.51 and 1.62 V, corresponding to Li-ion insertion/extraction to and from the LTO structure. The voltage gap between the anodic and cathodic peaks ($\Delta E_p$) of LTO-700 is only 0.11 V, which is much less than 0.22 V for LTO-800. In addition, the peak current density of LTO-700 is almost twice that of LTO-800. All these observations reflect the faster electrochemical reaction of the LTO-700 material compared to the LTO-800 material.

The XRD patterns, TEM and STEM images results demonstrate that the densely packed LTO-700 spheres consist of self-assembled nanocrystals with an average diameter ~42 nm, significantly smaller than that of the longer annealed LTO-800 spheres (~55 nm), resulting in a much higher grain boundary density in the LTO-700 material and suggesting that this is responsible for the longer cycle life and better capacity retention at high rates of the LTO-700 material.

To understand the origin of the improved performance, the electrochemical impedance spectra (EIS) of the electrodes at various SOC after 0.1 C and 10 C were measured (Figure 6a–d), which were simulated by the Z-view software using the equivalent circuit models (Figure S13 in the SI). The calculation of the Li-ion diffusion coefficients ($D_{Li}$) is shown in the SI (Figure S14 and Table S2). The obtained charge transfer resistance ($R_{ct}$) and $D_{Li}$ are shown in Figure 6e–h. It is seen that during the initial stage of lithiation at 0.1C, the $R_{ct}$ decreases rapidly when the voltage of the electrodes decreases from 1.9 to 1.6 V, an effect that appears stronger for LTO-700. From 5% to 95% SOC, $R_{ct}$ decreases slightly for LTO-700, reaching a smaller value before it increases again toward 100% SOC (Figure 6g). In comparison to LTO-800, the $D_{Li}$ of LTO-700 displays a large increase between 5% and 20% SOC, declining slightly between 20% and 95% SOC before it finally decreases again (Figure 6e). The Li-ion diffusion coefficient in LTO-700 at 52% SOC amounts $6.2 \times 10^{-12}$ $cm^2$ $s^{-1}$ after 0.1C cycling and $18.4 \times 10^{-12}$ $cm^2$ $s^{-1}$ after 10C cycling, significantly larger than that of the LTO nanosheets reported previously ($4.0 \times 10^{-13}$ $cm^2$ $s^{-1}$).[18] The large $D_{Li}$ of LTO-700 suggests a high ionic conductivity as can be derived by the Nernst–Einstein equation.[35,36] The present Li-ion diffusion coefficients derived from the EIS are in good agreement with those found by NMR, at room temperature $2.7 \times 10^{-12}$ $cm^2$ $s^{-1}$ [37,38] and $4.0 \times 10^{-12}$ $cm^2$ $s^{-1}$.[39] We anticipate that the small difference may be ascribed to the difference in the NMR and EIS techniques and/or differences in the LTO materials.

It is well-known that $R_{ct}$ is affected by both $D_{Li}$ and the electronic conductivity.[22,40] It is observed from Figure 6e that $D_{Li}$ increases only marginally when the SOC is below 5%. This suggests that the large decrease in $R_{ct}$ below 5% SOC is due to a dramatic increase of the electronic conductivity, in agreement with recent research in the initial stages of lithiation of LTO.[40]



DOI: 10.1021/acs.chemmater.5b02027
Chem. Mater. 2015, 27, 5647–5656

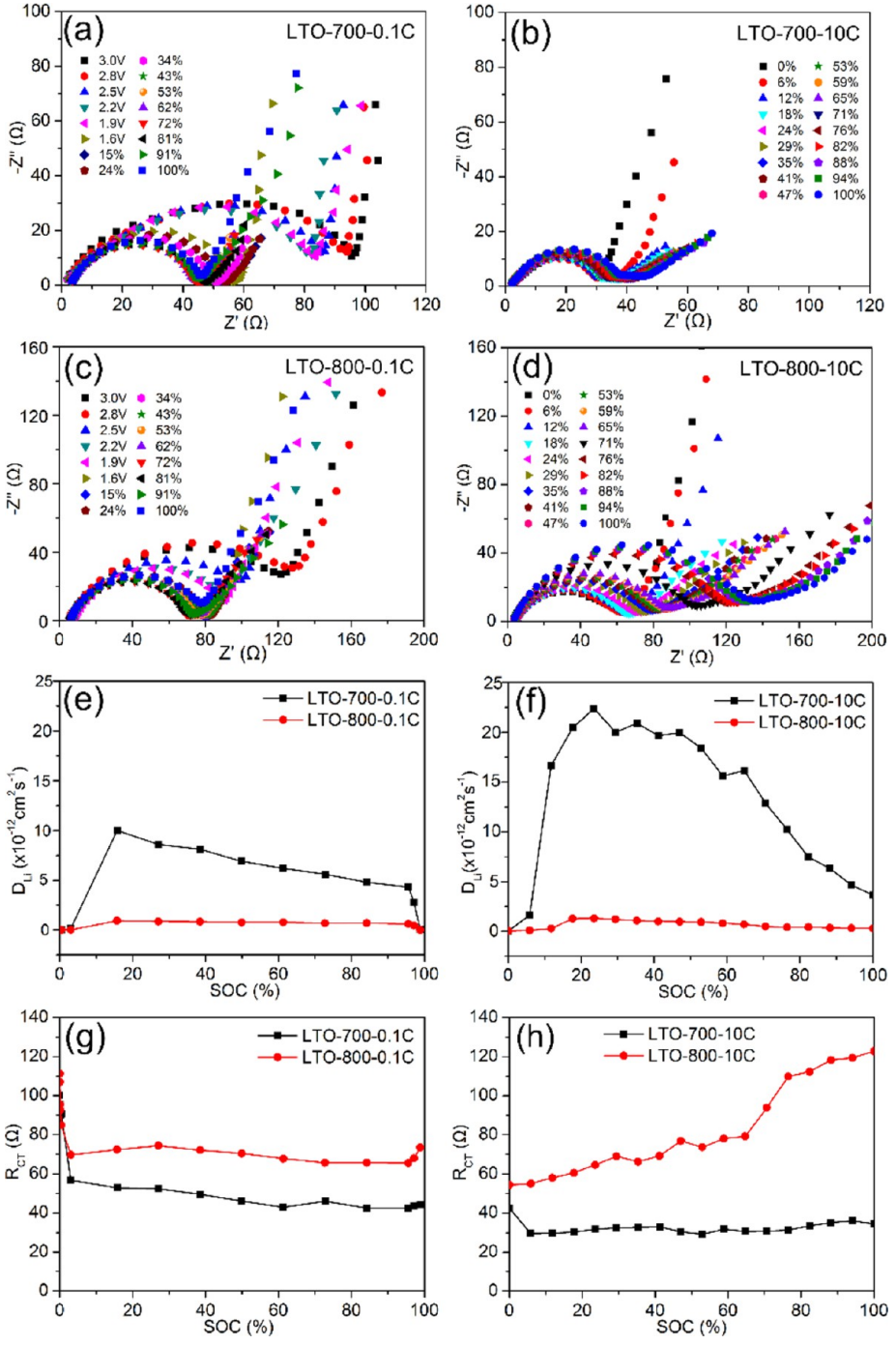


**Figure 6.** EIS of LTO-700(a, b) and LTO-800 (c, d) electrodes, and the $D_{Li}$ (e, f) and $R_{ct}$ (g, h) electrodes after lithiation to various SOC using 0.1 C and 10 C.

The thin carbon coating is expected to enhance the electronic transport between different submicron spheres, but the superior rate of densely packed LTO spheres suggests that the electrons can also easily enter the inside of the densely packed LTO spheres. It is well established that ion diffusion along the grain boundaries can be orders of magnitude faster than bulk diffusion through the grains[41] and that for LTO deviation from the end member compositions ($Li_4Ti_5O_{12}$ and $Li_7Ti_5O_{12}$) results in a dramatic increase in both Li-ion and electron mobility due to the availability of vacancies at the interfaces of Li 8a and 16c occupation.[38−40,42] A similar situation can be expected to occur at the grain boundaries, providing faster Li-ion and electron transport as compared to bulk LTO.[40,43] This suggests that in the initial stages of lithiation the grain boundary regions are lithiated first, as illustrated by Figure 7, creating a better electronically conducting network throughout the abundant grain boundaries in the compact LTO-700 spheres, explaining the larger decrease in $R_{ct}$ at low SOC. The mobile Li-ions in the grain boundary region initially form only a small fraction of the total amount of Li-ions, most of which will reside on bulk 8a sites having poor mobility,[39] explaining the small increase in the average $D_{Li}$ at low SOC. Between 5% and 95% SOC, this 3D charge transport network can be expected to induce more nanocrystals to transform within the compact


DOI: 10.1021/acs.chemmater.5b02027
Chem. Mater. 2015, 27, 5647−5656

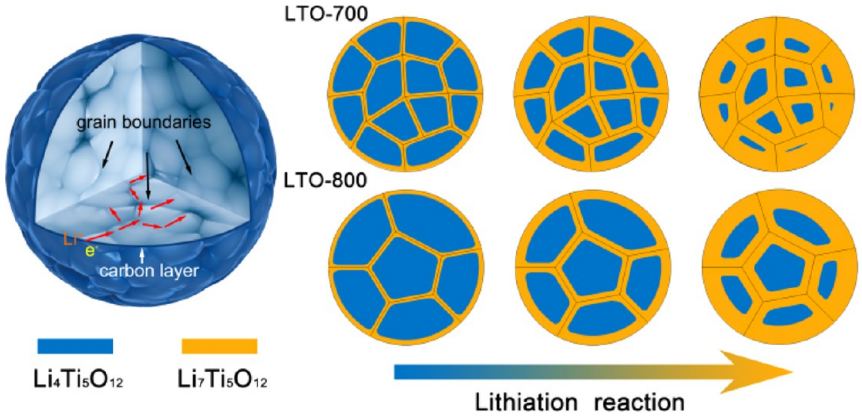


**Figure 7.** Schematic illustration of lithium ion diffusion along the grain boundaries in highly compact LTO spheres (red arrows: Li ion diffusion, black arrows: grain boundaries) and lithiation reaction process in LTO-700 and LTO-800 spheres (blue: $Li_4Ti_5O_{12}$, yellow: $Li_7Ti_5O_{12}$).

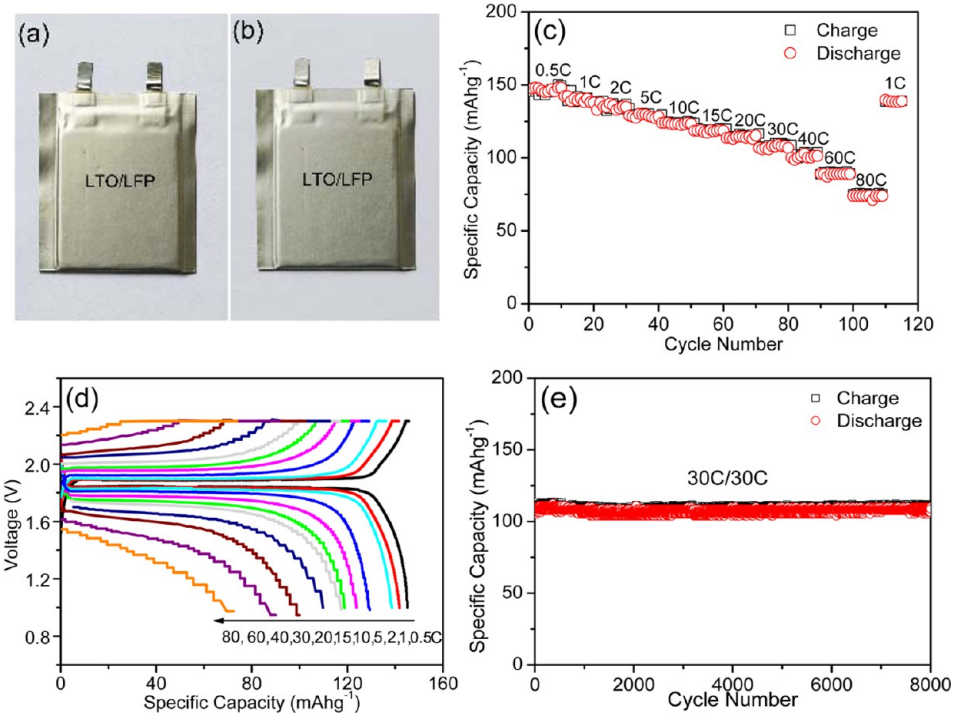


**Figure 8.** Photographs of LTO/LFP full cell (a) before and (b) after 8000 cyclic tests at current density of 30 C. (c) Specific capacities of LTO spheres and (d) the specific capacity vs voltage curves in full LFP/LTO batteries at various (dis)charge rates from 0.5 to 80 C, (e) cyclic performance at a rate of 30 C/30 C.

LTO-700 spheres, creating more phase boundaries where the Li-ion mobility is higher, rationalizing the much larger average diffusion coefficients observed in Figure 6e. In addition, the very steep increase in $D_{Li}$ upon lithiation starting at 5% SOC can be explained by recent NMR measurements that indicate a dramatic increase in Li-ion diffusivity already at very low Li compositions[42] as compared to the poor diffusivity of the end member phases $Li_4Ti_5O_{12}$ and $Li_7Ti_5O_{12}$.[37−39,42]

The EIS after 10 C cycling, Figure 6f and 6h, reveals a remarkable increase in $D_{Li}$ and a decrease in $R_{ct}$ for the LTO-700 material, not observed for LTO-800. It should be noted that after the 0.1 C and 10 C cycling to each SOC, the electrodes were rested for 2 h before the EIS was measured, and hence, the large difference in Li-ion diffusion coefficients between 0.1 C and 10 C implies a different distribution of Li-ions throughout the electrode materials resulting in more mobile Li-ions after 10 C cycling. A possible explanation is that more LTO grains are actively transforming at higher rates, as was recently shown to occur for $LiFePO_4$, a cathode Li-ion insertion electrode material.[44] More transforming grains will lead to extra interfaces between the end member phases resulting in more mobile charge carriers,[39,42] giving an explanation for the large diffusion coefficients after fast (10 C) cycling.

We conclude that the much better ionic and electronic transport properties of LTO-700 as compared to LTO-800 may be attributed to the grain boundary density. The more abundant grain boundaries in LTO-700 compared to LTO-800 will form a better interconnected 3D network for electron and Li-ion transport, explaining the much better performance at large (dis)charge rates. Compared to the much more porous nanosized LTO/Carbon composites, the present strategy leads


DOI: 10.1021/acs.chemmater.5b02027
Chem. Mater. 2015, 27, 5647−5656

to significantly larger tap densities and hence volumetric energy density, while maintaining efficient Li-ion transport. We believe that the concept of polycrystalline materials densely assembled by primary nanograins for combining large volumetric energy density and high rate performance provide a valuable and general strategy to enhance the performance of Li-ion electrode materials.

In order to evaluate the actual performance of LTO spheres in full battery, soft packed full LFP/LTO batteries were assembled using commercial LFP as cathode (Figure S15 in the SI) and LTO-700 spheres as anode. Figure 8 presents the photographs of LFP/LTO batteries and their rate performance and cyclic performance under same (dis)charge rates. It is observed that the specific capacities of the LTO spheres in LFP/LTO batteries at 0.5, 5, 10, 30, 60, and 80 C are 145.7, 129.3, 125.1, 110.1, 90.0, and 75.8 mAh $g^{-1}$. The specific capacities at 10 and 60 C remain to 85.9% and 61.8% of that achieved at 0.5 C. Again the LTO spheres exhibit excellent rate performance at ultrahigh (dis)charge rates in full LFP/LTO batteries. Interestingly, Figure 8c indicates that the LFP/LTO batteries almost do not show any capacity decay even after 8000 cycles at a (dis)charge rate of 30 C (the specific capacity of LTO at 30 C changes from 111.0 to 108.8 mAh $g^{-1}$) and the (dis)charge polarization does not increase during cycling (Figure S16 in the SI). These results indicate that the LTO-700 spheres poses remarkable cycling stability. In addition, it is observed from Figure 8a,b that the LFP/LTO batteries hardly causes gassing, most likely due to the minimization of the electrode−electrolyte interface.[34] This can be attributed to its unique structure with lower specific surface area and uniform carbon coating. The excellent electrochemical behavior in combination with the high volumetric capacity make the prepared compact LTO spheres a highly promising material for electric-powered vehicle applications.

## SUMMARY AND OUTLOOK

We have developed a facile one-pot in situ synthetic approach to produce compact spheres tightly grown by spinel LTO nanocrystals. The compact LTO spheres were formed after a simple hydrolysis reaction followed by a low temperature heat treatment, which does not require the more complex spray-drying or hydrothermal processes. The LTO spheres exhibit remarkable rate capabilities (e.g., 148.6 and 130.1 mAh $g^{-1}$ at 10 and 20 C, respectively) and very stable long-term capacity retention (e.g., 3% capacity loss after 500 cycles at 10 C in half cell and almost no capacity fading after 8000 cycles at 30 C in LFP/LTO batteries). Owing to the unique structure of the compact LTO spheres, consisting of densely packed primary LTO nanocrystals with a very low carbon content (∼0.4 wt %), the LTO spheres possess an exceptionally high tap density of 1.2 g $cm^{-3}$ and a small specific surface area of 8.6 $m^2$ $g^{-1}$, which are of considerable significance in achieving the LTO-based batteries with high volumetric energy densities. These findings highlight that high rate Li-ion and electron transport, comparable to that of porous or nanosheet structures with high carbon contents, can be achieved without compromising the volumetric energy density. The remarkable performance at fast cycling rates is due to the excellent electronic and Li-ion transport properties of the compact LTO spheres, explained by the large abundance of grain boundaries between the nanocrystals creating an interconnected 3D network for Li-ion and electron transport. Thereby, this study presents a universal method to design and prepare Li-ion electrode materials combining high rate performance with low carbon content and high tap density. These findings are of extensive general interest for the development of compact electrode materials as required for lithium ion power batteries with high volumetric energy densities.

## METHODS

The phase compositions of the prepared LTO spheres were measured by X-ray diffraction (XRD, Rigaku D/max 2500/PC using Cu K$\alpha$ radiation with $\lambda$ = 1.5418 Å). The morphologies and structures were examined by a field emission scanning electron microscope (FESEM, HITACH S4800) at 5 kV and a high resolution and scanning transmission electron microscope (HRTEM, STEM TECNAIG2 F30) at an accelerating voltage of 300 kV. The cross-section of LTO spheres was obtained by model E-3500 ion milling system. The Raman spectra were collected on a Raman Spectrometer (HORIBA Labram HR Evolution) with a 532 nm Ar-ion laser. The Fourier transform infrared spectroscopy (FTIR, Nicolet iS10) was measured in the near-infrared region. The carbon content was determined by a NETZSCH STA449F3 thermal analyzer. The electrical conductivities of LTO powders were measured using the four-point probe method (LORESTA GP, MCPT610). The nitrogen adsorption/desorption isotherms were obtained at 77 K by using an automated adsorption apparatus (Micromeritics ASAP 2020). The surface area was calculated on the basis of the Brunauer−Emmett−Teller (BET) equation.

Electrochemical measurements were performed by using CR2032 coin half-cells and full LFP/LTO batteries. The LTO electrodes were prepared by mixing the as-prepared LTO spheres with Super-P as conducting agent and polyvinylidene fluoride in an *N*-methylpyrrolidinone solution with an 80:10:10 weight ratio. The LTO electrode loading was 1.5 mg $cm^{-2}$ for half cells and 3.68 mg $cm^{-2}$ for full LFP/LTO cells. For the half-cell test, metallic lithium was used as the anode. The 1 M $LiPF_6$ solution in ethylene carbonate (EC)/diethyl carbonate (DEC)/ethyl methyl carbonate (EMC) (volume ratio: 1:1:1) was used as the electrolyte. Microporous polyethylene (Celgard 2500) served as the separator. The assembled half cells were galvanostatically cycled between 1.0 and 2.5 V (on a Land 2001A battery testing system) at different current densities (the current corresponding to 1 C is 175 mA $g^{-1}$ for LTO half and full cells) at room temperature. The electrochemical impedance spectra (EIS) of electrodes after lithiation to various SOC were obtained on a VMP3 multichannel electrochemical station in the frequency range of $10^{-2}$−$10^5$ Hz. A perturbation of 5 mV was applied. Cyclic voltammograms (CVs) were recorded using the same electrochemical workstation at a scan rate of 0.1 mV $s^{-1}$ in the range of 1.0−2.5 V.

In order to examine the performance of compact LTO spheres in practical full batteries, soft packed LFP/LTO batteries with a capacity of 60 mAh were assembled using the same LTO electrodes, electrolyte, and separator as the half cells. The LFP cathode consisted of 84 wt % commercial $LiFePO_4$, 10 wt % Super-P, and 6 wt % polyvinylidene fluoride. The rate and cycling performance of soft packed LFP/LTO batteries were tested between 1 and 2.3 V at 25 °C using a Land battery tester. The batteries were charged with a constant current-constant voltage (CC−CV) mode and discharged with CC mode. The cutoff current at CV charge is 12 mA (0.2 C).

## ASSOCIATED CONTENT

### Supporting Information

XRD patterns, SEM images, and the electrochemical performance of LTO-600 spheres; the morphologies of LTO spheres reported in references; SEM image of LTO synthesized without HDA and with CTAB; STEM images, TGA and Raman spectra of LTO-700 and LTO-800; SEM images and FTIR spectra of the LTO-700 spheres before and after 500 cycles; the (dis)charge curves of LTO-700 and LTO-800 at 0.1 C in the first, second and third cycles; CV curves of LTO spheres, SEM images, XRD pattern and rate performance of the cathode



DOI: 10.1021/acs.chemmater.5b02027
*Chem. Mater.* 2015, 27, 5647−5656

material $LiFePO_4$; dis(charge) curves of LTO/LFP full cells at 30 C. The Supporting Information is available free of charge on the ACS Publications website at DOI: 10.1021/acs.chemmater.5b02027.

## AUTHOR INFORMATION


### Corresponding Authors

*E-mail: he.yanbing@sz.tsinghua.edu.cn.
*E-mail: m.wagemaker@tudelft.nl.
*E-mail: libh@mail.sz.tsinghua.edu.cn.

### Author Contributions

⊥C.W. and S.W. contributed equally to this work.


### Notes

The authors declare no competing financial interest.

## ACKNOWLEDGMENTS

This work was supported by the National Key Basic Research Program of China (2014CB932400), the National Natural Science Foundation of China (51202121 and 51232005), and the Guangdong Province Innovation R&D Team Plan for Energy and Environmental Materials (2009010025).

## REFERENCES


(1) Dunn, B.; Kamath, H.; Tarascon, J.-M. Electrical energy storage for the grid: a battery of choices. *Science* **2011**, *334*, 928.

(2) Park, G.; Gunawardhana, N.; Nakamura, H.; Lee, Y.-S.; Yoshio, M. The study of electrochemical properties and lithium deposition of graphite at low temperature. *J. Power Sources* **2012**, *199*, 293.

(3) Zhang, S. S.; Xu, K.; Jow, T. R. The low temperature performance of Li-ion batteries. *J. Power Sources* **2003**, *115*, 137.

(4) Zhang, S. S.; Xu, K.; Jow, T. R. Study of the charging process of a $LiCoO_2$-based Li-ion battery. *J. Power Sources* **2006**, *160*, 1349.

(5) Bruce, P. G.; Scrosati, B.; Tarascon, J.-M. Nanomaterials for Rechargeable Lithium Batteries. *Angew. Chem., Int. Ed.* **2008**, *47*, 2930.

(6) Choi, N.-S.; Chen, Z.; Freunberger, S. A.; Ji, X.; Sun, Y.-K.; Amine, K.; Yushin, G.; Nazar, L. F.; Cho, J.; Bruce, P. G. Challenges Facing Lithium Batteries and Electrical Double-Layer Capacitors. *Angew. Chem., Int. Ed.* **2012**, *51*, 9994.

(7) Park, K.-S.; Benayad, A.; Kang, D.-J.; Doo, S.-G. Nitridation-driven conductive $Li_4Ti_5O_{12}$ for lithium ion batteries. *J. Am. Chem. Soc.* **2008**, *130*, 14930.

(8) Liu, M.; Sun, J. In situ growth of monodisperse $Fe_3O_4$ nanoparticles on graphene as flexible paper for supercapacitor. *J. Mater. Chem. A* **2014**, *2*, 12068.

(9) Borghols, W. J. H.; Wagemaker, M.; Lafont, U.; Kelder, E. M.; Mulder, F. M. Size Effects in the $Li_{4+x}Ti_5O_{12}$ Spinel. *J. Am. Chem. Soc.* **2009**, *131*, 17786.

(10) Sun, Y.; Zhao, L.; Pan, H.; Lu, X.; Gu, L.; Hu, Y.-S.; Li, H.; Armand, M.; Ikuhara, Y.; Chen, L.; Huang, X. Direct atomic-scale confirmation of three-phase storage mechanism in $Li_4Ti_5O_{12}$ anodes for room-temperature sodium-ion batteries. *Nat. Commun.* **2013**, *4*, 1870.

(11) Lu, X.; Zhao, L.; He, X.; Xiao, R.; Gu, L.; Hu, Y.-S.; Li, H.; Wang, Z.; Duan, X.; Chen, L.; Maier, J.; Ikuhara, Y. Lithium Storage in $Li_4Ti_5O_{12}$ Spinel: The Full Static Picture from Electron Microscopy. *Adv. Mater.* **2012**, *24*, 3233.

(12) Li, N.; Zhou, G.; Li, F.; Wen, L.; Cheng, H.-M. A Self-Standing and Flexible Electrode of $Li_4Ti_5O_{12}$ Nanosheets with a N-Doped Carbon Coating for High Rate Lithium Ion Batteries. *Adv. Funct. Mater.* **2013**, *23*, 5429.

(13) Kang, E.; Jung, Y. S.; Kim, G.-H.; Chun, J.; Wiesner, U.; Dillon, A. C.; Kim, J. K.; Lee, J. Highly Improved Rate Capability for a Lithium-Ion Battery Nano-$Li_4Ti_5O_{12}$ Negative Electrode via Carbon-Coated Mesoporous Uniform Pores with a Simple Self-Assembly Method. *Adv. Funct. Mater.* **2011**, *21*, 4349.

(14) Shen, L.; Li, H.; Uchaker, E.; Zhang, X.; Cao, G. General Strategy for Designing Core−Shell Nanostructured Materials for High-Power Lithium Ion Batteries. *Nano Lett.* **2012**, *12*, 5673.

(15) Zhang, B.; Yu, Y.; Liu, Y.; Huang, Z.-D.; He, Y.-b.; Kim, J.-K. Percolation threshold of graphene nanosheets as conductive additives in Li 4 Ti 5 O 12 anodes of Li-ion batteries. *Nanoscale* **2013**, *5*, 2100.

(16) Zhang, B.; Huang, Z.-D.; Oh, S. W.; Kim, J.-K. Improved rate capability of carbon coated $Li_{3.9}Sn_{0.1}Ti_5O_{12}$ porous electrodes for Li-ion batteries. *J. Power Sources* **2011**, *196*, 10692.

(17) Feckl, J. M.; Fominykh, K.; Doblinger, M.; Fattakhova-Rohlfing, D.; Bein, T. Nanoscale porous framework of lithium titanate for ultrafast lithium insertion. *Angew. Chem., Int. Ed.* **2012**, *51*, 7459.

(18) Wang, Y. Q.; Gu, L.; Guo, Y. G.; Li, H.; He, X. Q.; Tsukimoto, S.; Ikuhara, Y.; Wan, L. J. Rutile-$TiO_2$ nanocoating for a high-rate $Li_4Ti_5O_{12}$ anode of a lithium-ion battery. *J. Am. Chem. Soc.* **2012**, *134*, 7874.

(19) Liu, J.; Song, K.; van Aken, P. A.; Maier, J.; Yu, Y. Self-Supported $Li_4Ti_5O_{12}$-C Nanotube Arrays as High-Rate and Long-Life Anode Materials for Flexible Li-Ion Batteries. *Nano Lett.* **2014**, *14*, 2597.

(20) Shen, L.; Uchaker, E.; Zhang, X.; Cao, G. Hydrogenated $Li_4Ti_5O_{12}$ nanowire arrays for high rate lithium ion batteries. *Adv. Mater.* **2012**, *24*, 6502.

(21) Yu, L.; Wu, H. B.; Lou, X. W. Mesoporous $Li_4Ti_5O_{12}$ hollow spheres with enhanced lithium storage capability. *Adv. Mater.* **2013**, *25*, 2296.

(22) Zhao, L.; Hu, Y. S.; Li, H.; Wang, Z.; Chen, L. Porous $Li_4Ti_5O_{12}$ coated with N-doped carbon from ionic liquids for Li-ion batteries. *Adv. Mater.* **2011**, *23*, 1385.

(23) Amine, K.; Belharouak, I.; Chen, Z.; Tran, T.; Yumoto, H.; Ota, N.; Myung, S. T.; Sun, Y. K. Nanostructured anode material for high-power battery system in electric vehicles. *Adv. Mater.* **2010**, *22*, 3052.

(24) Li, B.; Han, C.; He, Y.-B.; Yang, C.; Du, H.; Yang, Q.-H.; Kang, F. Facile synthesis of $Li_4Ti_5O_{12}$/C composite with super rate performance. *Energy Environ. Sci.* **2012**, *5*, 9595.

(25) Singh, D. P.; Mulder, F. M.; Wagemaker, M. Templated spinel $Li_4Ti_5O_{12}$ Li-ion battery electrodes combining high rates with high energy density. *Electrochem. Commun.* **2013**, *35*, 124.

(26) Singh, D. P.; Mulder, F. M.; Abdelkader, A. M.; Wagemaker, M. Facile Micro Templating $LiFePO_4$ Electrodes for High Performance Li-Ion Batteries. *Adv. Energy Mater.* **2013**, *3*, 572.

(27) Fongy, C.; Jouanneau, S.; Guyomard, D.; Badot, J. C.; Lestriez, B. Electronic and Ionic Wirings Versus the Insertion Reaction Contributions to the Polarization in $LiFePO_4$ Composite Electrodes. *J. Electrochem. Soc.* **2010**, *157*, A1347.

(28) Chen, D.; Cao, L.; Huang, F.; Imperia, P.; Cheng, Y.-B.; Caruso, R. A. Synthesis of Monodisperse Mesoporous Titania Beads with Controllable Diameter, High Surface Areas, and Variable Pore Diameters (14−23 nm). *J. Am. Chem. Soc.* **2010**, *132*, 4438.

(29) Monnier, A.; Schüth, F.; Huo, Q.; Kumar, D.; Margolese, D.; Maxwell, R. S.; Stucky, G. D.; Krishnamurty, M.; Petroff, P.; Firouzi, A.; Janicke, M.; Chmelka, B. F. Cooperative Formation of Inorganic-Organic Interfaces in the Synthesis of Silicate Mesostructures. *Science* **1993**, *261*, 1299.

(30) He, Y.-B.; Ning, F.; Li, B.; Song, Q.-S.; Lv, W.; Du, H.; Zhai, D.; Su, F.; Yang, Q.-H.; Kang, F. Carbon coating to suppress the reduction decomposition of electrolyte on the $Li_4Ti_5O_{12}$ electrode. *J. Power Sources* **2012**, *202*, 253.

(31) Yuan, T.; Yu, X.; Cai, R.; Zhou, Y.; Shao, Z. Synthesis of pristine and carbon-coated $Li_4Ti_5O_{12}$ and their low-temperature electrochemical performance. *J. Power Sources* **2010**, *195*, 4997.

(32) Aurbach, D.; Daroux, M. L.; Faguy, P. W.; Yeager, E. Identification of Surface Films Formed on Lithium in Propylene Carbonate Solutions. *J. Electrochem. Soc.* **1987**, *134*, 1611.

(33) Han, C.; He, Y.-B.; Li, B.; Li, H.; Ma, J.; Du, H.; Qin, X.; Yang, Q.-H.; Kang, F. Highly Crystalline Lithium Titanium Oxide Sheets Coated with Nitrogen-Doped Carbon enable High-Rate Lithium-Ion Batteries. *ChemSusChem* **2014**, *7*, 2567.




DOI: 10.1021/acs.chemmater.5b02027
*Chem. Mater.* 2015, 27, 5647−5656

(34) He, Y.-B.; Li, B.; Liu, M.; Zhang, C.; Lv, W.; Yang, C.; Li, J.; Du, H.; Zhang, B.; Yang, Q.-H.; Kim, J.-K.; Kang, F. Gassing in $Li_4Ti_5O_{12}$-based batteries and its remedy. *Sci. Rep.* **2012**, *2*, Article no. 913.
(35) Bai, Y.-J.; Gong, C.; Qi, Y.-X.; Lun, N.; Feng, J. Excellent long-term cycling stability of La-doped $Li_4Ti_5O_{12}$ anode material at high current rates. *J. Mater. Chem.* **2012**, *22*, 19054.
(36) Noda, A.; Hayamizu, K.; Watanabe, M. Pulsed-Gradient Spin−Echo 1H and 19F NMR Ionic Diffusion Coefficient, Viscosity, and Ionic Conductivity of Non-Chloroaluminate Room-Temperature Ionic Liquids. *J. Phys. Chem. B* **2001**, *105*, 4603.
(37) Wilkening, M.; Amade, R.; Iwaniak, W.; Heitjans, P. Ultraslow Li diffusion in spinel-type structured $Li_4Ti_5O_{12}$ - A comparison of results from solid state NMR and impedance spectroscopy. *Phys. Chem. Chem. Phys.* **2007**, *9*, 1239.
(38) Wilkening, M.; Iwaniak, W.; Heine, J.; Epp, V.; Kleinert, A.; Behrens, M.; Nuspl, G.; Bensch, W.; Heitjans, P. Microscopic Li self-diffusion parameters in the lithiated anode material $Li_{4+x}Ti_5O_{12}$ ($0 \leq x \leq 3$) measured by Li-7 solid state NMR. *Phys. Chem. Chem. Phys.* **2007**, *9*, 6199.
(39) Wagemaker, M.; van Eck, E. R. H.; Kentgens, A. P. M.; Mulder, F. M. Li-Ion Diffusion in the Equilibrium Nanomorphology of Spinel $Li_{4+x}Ti_5O_{12}$. *J. Phys. Chem. B* **2009**, *113*, 224.
(40) Kim, C.; Norberg, N. S.; Alexander, C. T.; Kostecki, R.; Cabana, J. Mechanism of Phase Propagation During Lithiation in Carbon-Free $Li_4Ti_5O_{12}$ Battery Electrodes. *Adv. Funct. Mater.* **2013**, *23*, 1214.
(41) Rahman, M. M.; Wang, J.-Z.; Hassan, M. F.; Wexler, D.; Liu, H. K. Amorphous Carbon Coated High Grain Boundary Density Dual Phase $Li_4Ti_5O_{12}$-$TiO_2$: A Nanocomposite Anode Material for Li-Ion Batteries. *Adv. Energy Mater.* **2011**, *1*, 212.
(42) Schmidt, W.; Bottke, P.; Sternad, M.; Gollob, P.; Hennige, V.; Wilkening, M. Small Change-Great Effect: Steep Increase of Li Ion Dynamics in $Li_4Ti_5O_{12}$ at the Early Stages of Chemical Li Insertion. *Chem. Mater.* **2015**, *27*, 1740.
(43) Song, M.-S.; Benayad, A.; Choi, Y.-M.; Park, K.-S. Does $Li_4Ti_5O_{12}$ need carbon in lithium ion batteries? Carbon-free electrode with exceptionally high electrode capacity. *Chem. Commun.* **2012**, *48*, 516.
(44) Li, Y.; El Gabaly, F.; Ferguson, T. R.; Smith, R. B.; Bartelt, N. C.; Sugar, J. D.; Fenton, K. R.; Cogswell, D. A.; Kilcoyne, A. L. D.; Tyliszczak, T.; Bazant, M. Z.; Chueh, W. C. Current-induced transition from particle-by-particle to concurrent intercalation in phase-separating battery electrodes. *Nat. Mater.* **2014**, *13*, 1149.



DOI: 10.1021/acs.chemmater.5b02027
*Chem. Mater.* 2015, 27, 5647−5656